A horn-reflector antenna for high-performance submillimetre-wave applications

S. Withington, G. Yassin, M.Buffey, and C. Norden
Cavendish Laboratory, Madingley Road, Cambridge, CB3 OHE, UK

1 Introduction

In recent years, it has become clear that the submillimetre-wave part of the electromagnetic spectrum contains a wealth of information about the state and distribution of molecular and ionised gas in distant galaxies. Unfortunately, the spectral lines associated with these objects are broad and faint, and therefore particular care is required to ensure that they can be detected, and where appropriate mapped, in an efficient and straightforward manner. The design of extragalactic imaging arrays, as opposed to galactic imaging arrays, has already been considered in some detail [1]. The important point is that the performance of individual pixels—noise temperature, bandwidth, aperture efficiency, stability, freedom from systematic baseline effects, etc.—should not be compromised merely in order to build an array. Indeed, what is required is a small, linear array of extremely high-performance detectors. In this paper, we describe a horn-reflector antenna which is ideal for small-format, high-performance imaging applications.

2 Basic arrangement

The basic imaging array is shown in Fig. 1. Each pixel consists of a corrugated horn and a 90° offset parabolic reflector. In a conventional antenna the reflector is illuminated by the far field of a diffraction-limited horn; whereas in our arrangement the reflector is illuminated by the near field of a large-flare-angle horn. This combination allows a flat, tapered field to be produced which is many wavelengths in diameter. The design of each element is similar to that of the Hogg horn where a parabolic reflector is placed at the aperture of a pyramidal horn. Clearly, the horn-mirror combination will generate amplitude distortions and a cross-polarised field; in this paper, we consider how strongly these effects depend on the flare angle of the horn and consequently on the depth of the mirror. Obviously, there are subtle differences in performance depending on how the polarisation of the horn is orientated with respect to the mirror. In our design, the E-vector is parallel to the symmetry axis of the mirror, although the other polarisation can easily be analysed by using the procedure described here.

A key feature of the arrangement is that highly-collimated beams can be produced without the use of plastic lenses. As a consequence, the design gives high beam efficiency, low far-out scattering, and low cross polarisation. It eliminates the troublesome standing

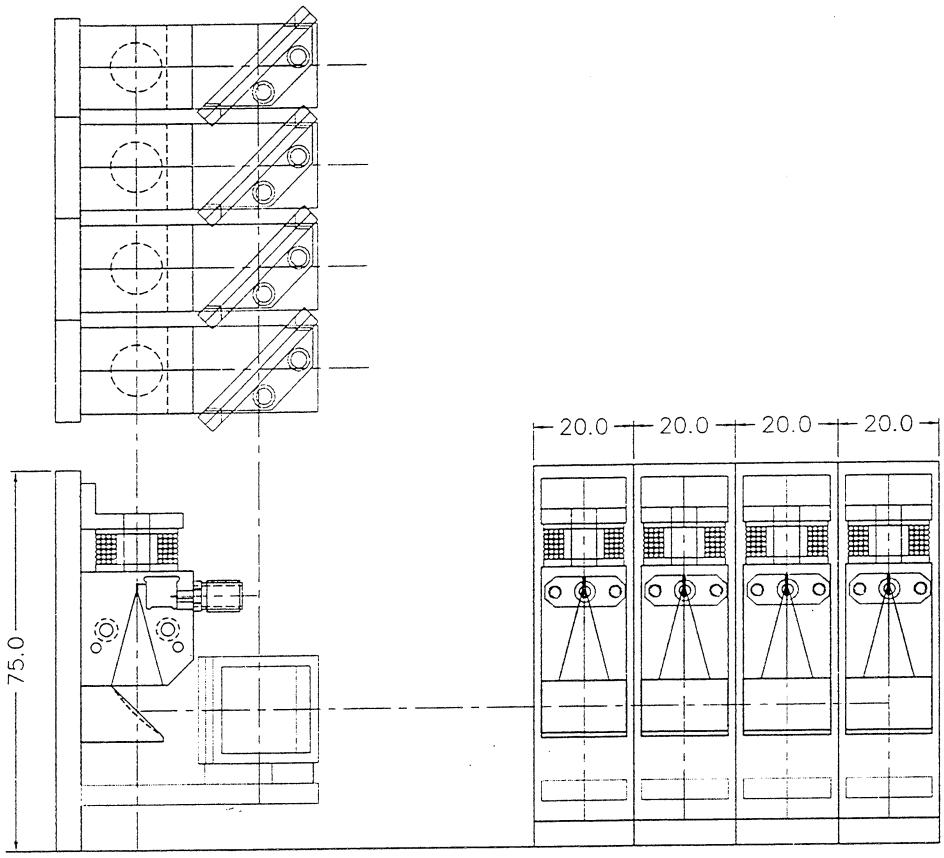

Figure 1: A linear imaging array based on horn-reflector antennas. The dimensions shown are in millimetres.

waves that are caused by dielectric interfaces, it is compact, and it is straightforward to design and manufacture. It should be appreciated that the generation of far-out sidelobes, due to diffraction at the edges of the mirror, is extremely small due to the field in the projected aperture plane being highly tapered. Moreover, the far-out sidelobes associated with the real aperture can, for all practical purposes, be completely eliminated by machining grooves into the front face of the block [2]. The only other potential problem is the generation of high-order modes in the horn itself; it is well known, however, that with careful design these can be avoided.

3 Calculation of aperture-plane fields

The configuration was analysed by using geometrical optics between the mouth of the horn and the projected aperture plane, and a Gaussian-mode expansion beyond. This approach assumes that the flare angle of the horn is sufficiently large that diffraction does not occur in the region occupied by the mirror. This assumption is in accordance with our desire to use a compact horn to generate a highly-collimated beam.

There are various ways in which the geometrical projection could have been achieved.

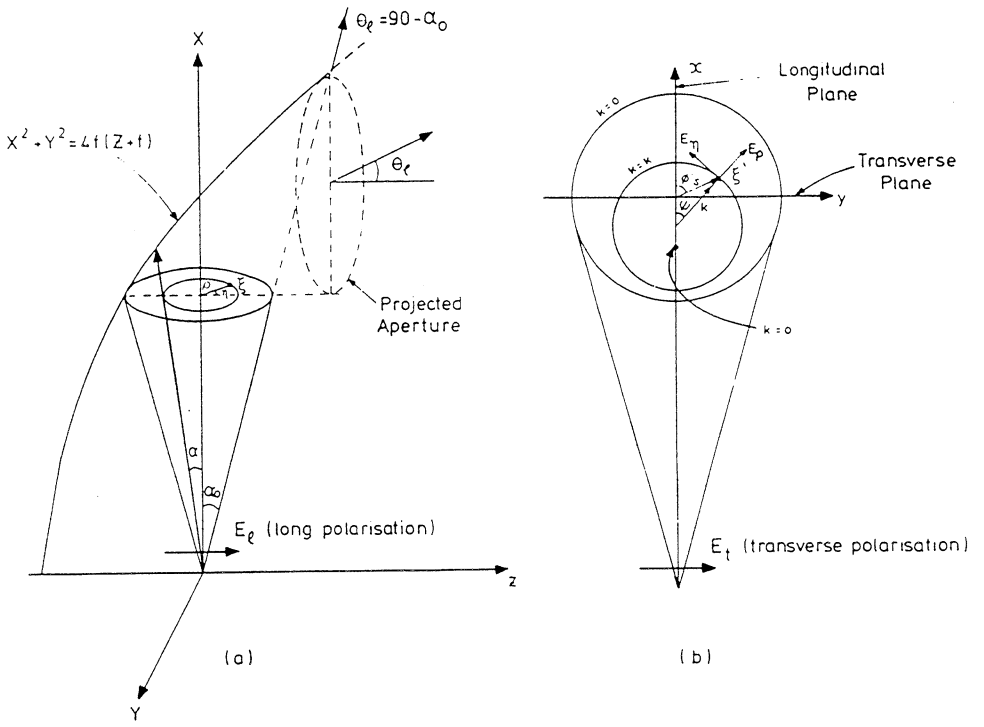

Figure 2: The geometry of the projected aperture.

Here we recognise that if the apex of the horn is located at the focal point of the mirror, the polar coordinate system at the aperture of the horn is transformed into a bipolar coordinate system at the projected aperture plane [3]: see Fig. 2. The mapping is therefore conformal. To see how this works, first of all recognise that the equation describing the paraboloidal reflector is

$$X^2 + Y^2 = 4f(Z+f) \tag{1}$$

and the equation describing concentric conical surfaces radiating from the aperture of the horn is

$$Y^2 + Z^2 = K^2 X^2 \ , \tag{2}$$

where $K = \tan\alpha$ and α is the semi-flare angle of the cone. By combining these equations and eliminating Z it is possible to derive expressions for the intersections of the cones and the paraboloidal reflector. Loci of constant radii, ρ, are transformed according to

$$\left[X - 2f\left(K^2+1\right)^{1/2}\right]^2 + Y^2 = 4f^2K^2 \ , \tag{3}$$

which is a circle of centre

$$C_K = 2f\left(K^2+1\right)^{1/2} \tag{4}$$

and radius

$$R = 2fK \ . \tag{5}$$

Hence the paraboloidal reflector transforms a family of concentric circles in the $Y-Z$ plane into a family of non-concentric circles in the $X-Y$ plane. Similarly, it can be shown that loci of constant azimuthal angle, η, are transformed according to

$$X^2 + (Y - 2f\cot\eta)^2 = 4f^2\csc^2\eta \tag{6}$$

which again is a family of circles. Hence, a family of radial lines in the $Y-Z$ plane transforms into a family of circles in the $X-Y$ plane.

A key parameter in the above equations is the focal length of the paraboloid f. This parameter can be found by noting that the vertex of the paraboloid is one focal length away from the apex of the horn. Hence,

$$f = \frac{a + (a^2 + l^2)^{1/2}}{2} \tag{7}$$

where a is the radius of the aperture of the horn, and l is the length of the horn. Also, we can find the radius of the projected circle corresponding the full semi-flare angle of the horn, $\alpha_o = \tan^{-1}(a/l)$, and combine it with the above equation for the focal length to show that there is a magnification of

$$M = \frac{1 + \cos\alpha_o}{\sin\alpha_o} \tag{8}$$

in the horn-reflector combination. This magnification is of considerable benefit in helping to produce a highly-collimated beam. For a semi-flare angle of 15° the magnification factor is 1.3, which is appreciable.

To enable far-field beam patterns to be calculated, it is convenient to express the co-polar and cross-polar fields in the projected aperture plane in terms of a cartesian coordinate system. We therefore set up a cartesian system centred on the point corresponding to the centre of the image of the aperture of the horn. It is straightforward to show that

$$y = Y \tag{9}$$

and

$$x = X - C_{K_o} = X - 2f\left(K_o^2 + 1\right)^{1/2} . \tag{10}$$

We now wish to derive expressions for the co-polar and cross-polar components of the scattered field in this new coordinate system. If E_ρ and E_η are the field components in the aperture of the horn, then we have for a corrugated horn

$$E_\rho = J_o(w)\cos(\eta) \tag{11}$$

and

$$E_\eta = -J_o(w)\sin(\eta) . \tag{12}$$

In these equations, $J_o(w)$ is the zero-order Bessel function, $w = 2.405K/K_o$, and it is assumed that the horn is polarised along the symmetry axis of the mirror. Moreover, if E_x and E_y are the Cartesian components of the field in the projected aperture plane, then

$$E_x = \frac{1}{d}\left[E_\rho\cos(\psi) + E_\eta\sin(\psi)\right] \tag{13}$$

and

$$E_y = \frac{1}{d}\left[E_\rho \sin(\psi) - E_\eta \cos(\psi)\right] \tag{14}$$

where ψ is the angle shown in Fig. 2, and d, which accounts for the attenuation suffered by the spherical wave, is the distance from the apex of the horn to the reflector.

Although, the principle by which the projection is determined is straightforward, it is surprisingly awkward to accumulate all of the information that is necessary to construct the field components [4]. Particular care must be taken to ensure that the angles are handled correctly.

4 Calculation of radiated fields

For compatibility with Gaussian Optics, we expand the co-polar and cross-polar fields in the projected aperture plane as sums of Gaussian-Hermite modes:

$$E(x,y,z) = \sum_{m,n} A_{m,n}\psi_{m,n}(x,y,z) \ , \tag{15}$$

where we have one set of mode coefficients for each polarisation. The individual modes are described by

$$\begin{aligned}\psi(x,y,z) \ = \ & \frac{\sqrt{2}}{w(z)} h_m\left[\frac{\sqrt{2}x}{w(z)}\right] h_n\left[\frac{\sqrt{2}y}{w(z)}\right] \\ & \exp\left[j(m+n+1)\tan\left(\frac{z}{z_c}\right)\right] \exp\left[\frac{-j\pi\left(x^2+y^2\right)}{\lambda R(z)}\right] \exp\left[-jkz\right]\end{aligned} \tag{16}$$

where

$$h_m(u) = \frac{H_m(u)e^{-u^2/2}}{\left(\sqrt{\pi}2^m m!\right)^{1/2}} \tag{17}$$

and $H_m(u)$ is the Hermite polynomial of order m in u; $h_m(u)$ is an orthonormal set of functions. The symbols have their usual meanings, and

$$z_c = \frac{w_o^2\pi}{\lambda} \tag{18}$$

is the confocal distance. The mode coefficients are easily determined by evaluating the overlap integrals over the projected aperture plane. Moreover, because the phase is flat at that plane, the overlap integrals are real:

$$A_{mn} = \int_{-\infty}^{+\infty} E(x,y,0)\frac{\sqrt{2}}{w_o} h_m\left[\frac{\sqrt{2}x}{w_o}\right] h_n\left[\frac{\sqrt{2}y}{w_o}\right] \ . \tag{19}$$

Once the mode coefficients are known it is straightforward to reconstruct the field at any plane in the beam.

In principle, when selecting the mode set, it is possible to choose the beam waist, w_o, and the maximum number of modes, N, in an arbitrary manner. In practice, the choice will affect the efficiency with which the summations converge. It is usual practice to use the

waist that places most of the power in the lowest-order mode and to terminate the sum at some suitably-large mode number. Here, we could adopt this procedure by using the waist that is appropriate for a corrugated horn, and taking into account the magnification in the horn-reflector combination. Because, however, the projected aperture is many wavelengths in size, it is much more efficient to use a mode set that is based on the eigenfunctions of the optical system being considered [5]. In fact, we choose the waist according to

$$w_o = \left[\frac{\lambda s}{2\pi \tan\theta}\right]^{1/2} \tag{20}$$

where $s = Ma$ is the half side length of the projected aperture plane and θ is the maximum angular field of view. The number of modes is then given by

$$N = \left[\frac{s\pi \tan\theta}{2\lambda}\right] . \tag{21}$$

In reality, we use about twice this number to get exceptionally-good beam patterns.

5 Simulations

To verify the above theory, we calculated the beam patterns of a horn-reflector antenna, which was developed originally for microwave background measurements over the frequency range 12-18GHz [4]. The system was designed to give a 2° beamwidth at 17GHz. The semi-flare angle of the horn was 15°, the diameter 52cm, and the length 97cm. According to the above formulas, the focal length of the mirror was 63cm, and the magnification factor 1.3.

The beam patterns of the horn were originally measured by using a rotating table mounted at 3m above the ground. A pyramidal horn was then placed on a hill 70m from the antenna. This large distance was needed to ensure that the measurement plane was in the far field of the beam. Examples of the main beam measurements are shown in Fig. 3 where theoretical curves based on the above analysis have been included. Clearly, the beam patterns are in precise agreement with the theory. The precise agreement between the calculated and measured cross-polar patterns is particularly satisfying.

Having verified the basic theory, we can now investigate how large the flare angle of the horn can be made before amplitude distortion and cross-polar scattering become a problem. In Figs. 4-6, we show the aperture distributions and far-field beam patterns of three, 345GHz, horns having different dimensions. In this sequence of plots, the aperture radius was held constant at 5mm and the length of the horn was increased from 5mm to 20mm. These dimensions correspond to sizes typical of a 345GHz imaging array. Clearly, as the horn becomes longer, the cross-polar scattering and the amplitude distortions become less. At 20mm, the cross-polar scattering is at an acceptable level and the central region of the beam pattern corresponds exactly to that of a corrugated horn. The flare angle of the horn is 15°, which is the same as the one measured above.

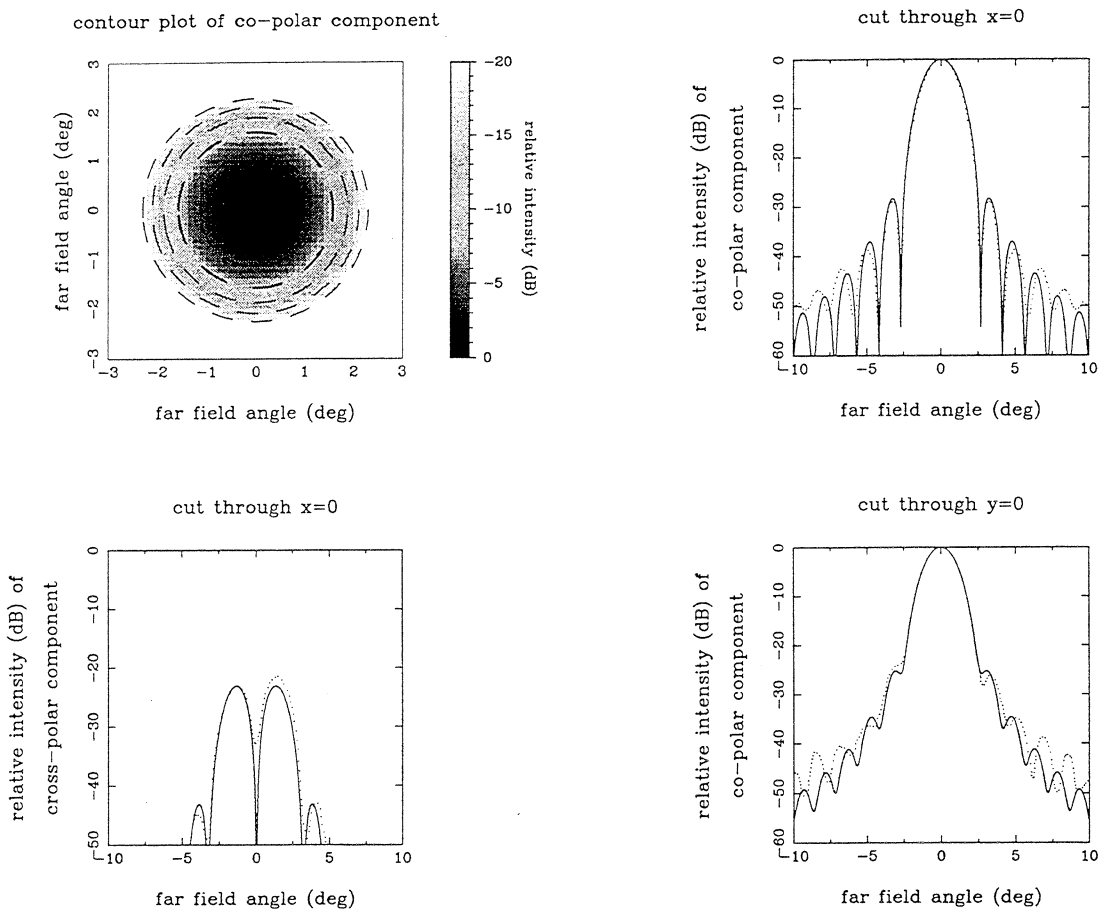

Figure 3: The experimental and theoretical performance of the 17GHz horn-reflector described in the text. The horn is polarised in the longitudinal direction, and the co-polar and cross-polar far-field beam patterns are shown.

6 Fabrication techniques

Because the aim of the work is to fabricate high-performance linear arrays, perhaps of up to eight elements long, it is important that the individual antennas are easy to manufacture. The paraboloidal mirrors are easy to produce in volume, because they can be diamond turned all at the same time. Producing eight corrugated horns is, however, more difficult. A further restriction is that, because of weight, we wished to manufacture the horns out of aluminium. Obviously, it is not possible to electroform aluminium horns, and therefore some other manufacturing method had to be found.

In pursuit of the above ideals, we developed a technique that allows a corrugated horn to be machined directly into a split aluminium block. Essentially, the work is held fixed on the slide of a lathe. The advantage of not rotating the work is that the cutting process can be observed through a binocular microscope. The tool is held in a boring head which rotates in the jaws of the lathe. The actual cutting surface is at right angles to the plane of rotation. If the boring head is driven out as the workpiece is moved along, a conical horn is manufactured. Indeed this operation is the first step in manufacturing a corrugated horn. The appropriate synchronization is achieved by a simple gearing mechanism on the

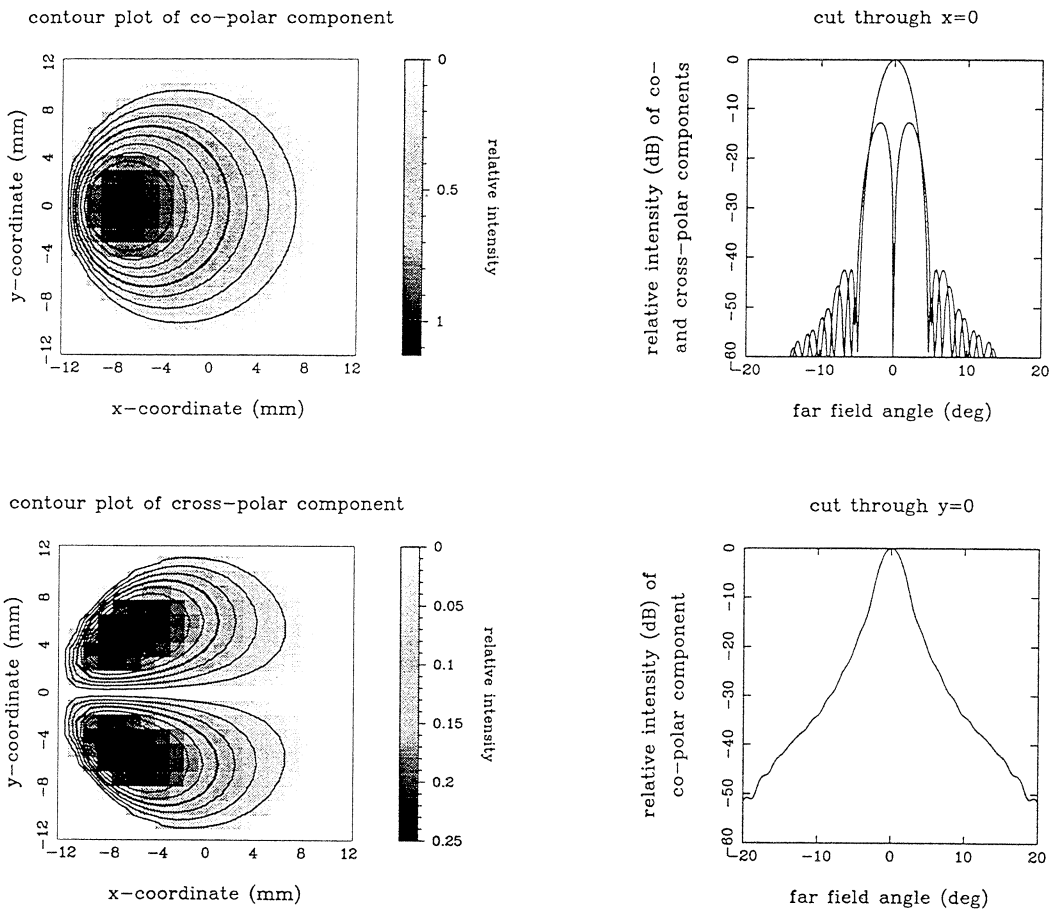

Figure 4: The co-polar and cross-polar fields in the projected aperture of a 345GHz horn having an aperture radius of 5mm and a length of 5mm. The co-polar and cross-polar far-field power patterns are also shown.

boring head, which forces the tool to move out by a certain amount on each rotation. The horn, is of course, manufactured in two halves, and the cone is cut after the waveguide, complete with backshort, is routed into the block.

To cut a corrugation the longitudinal position of the work is held fixed and the work is driven on axis. The position of the boring head determines the depth of the groove. In actual fact this operation is performed by a small DC motor which drives the work in slowly and then automatically retracts the work at speed after the groove has been cut. The change in direction is initiated by an ordinary microswitch, and we have found that accuracies of 2μm can routinely be achieved. Clearly, the depth and position of each slot are determined by the position of the boring head and lead screw respectively. By using toothed wheels these can be set easily and accurately. Hence the procedure needed to cut a groove is merely to click the two toothed wheels on one position and then press a button which initiates the cutting operation.

Various problems had to be solved before the process became reliable. For example, a problem was found to occur when swarf was left on the surface of the block. The swarf could be picked up by the tool prior to cutting, and this tended to push the thin walls of the corrugations over to one side. By allowing a small amount cutting fluid to flow over

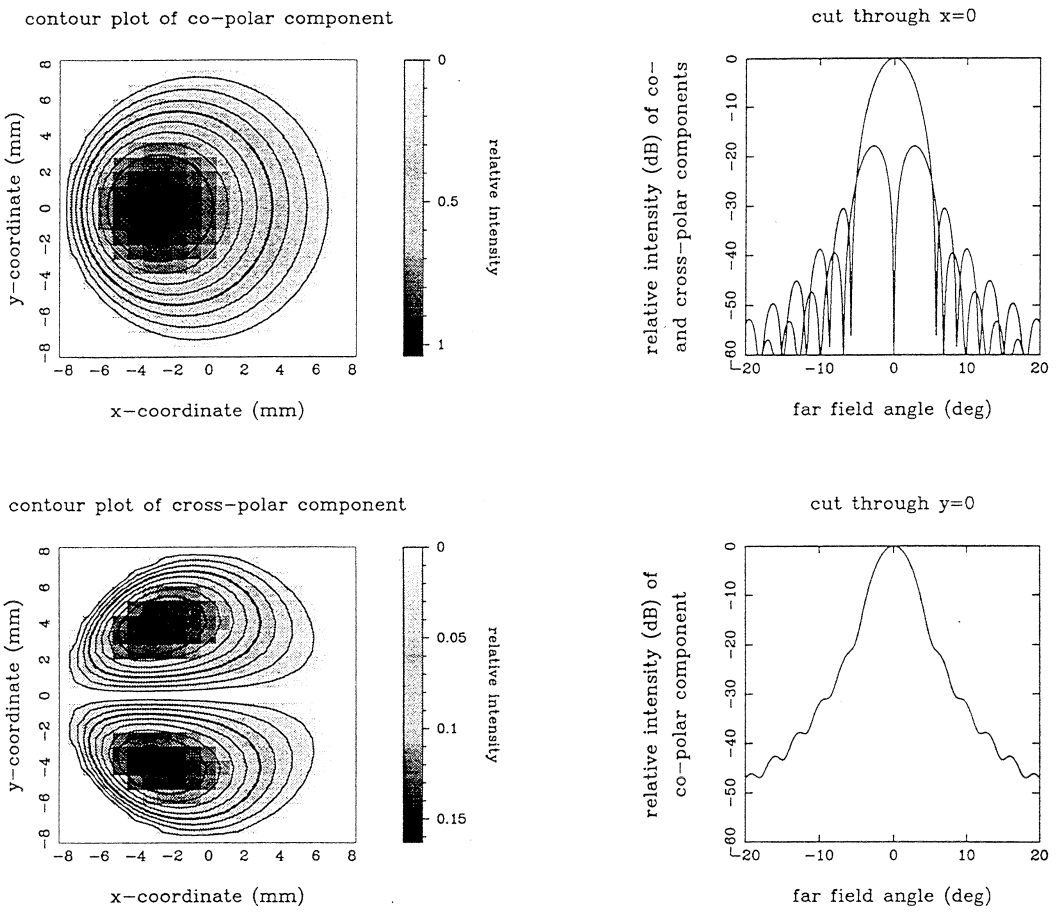

Figure 5: The co-polar and cross-polar fields in the projected aperture of a 345GHz horn having an aperture radius of 5mm and a length of 10mm. The co-polar and cross-polar far-field power patterns are also shown.

the surface of the block this problem was completely eliminated.

The main difficulty in developing the manufacturing process was to work out how the tools should be made. Three tools are now used: The first one is used for cutting the conical horn and has to be small enough to fit inside the waveguide. The second one is used for cutting the first few deep slots (aspect ratio 3:1) and is made of molybdenum tool steel for strength. Unfortunately, this material wears quickly and is not used for cutting the large number of shallow slots. The third tool is used for cutting the less deep slots. It is made of tungsten carbide which is brittle but wears slowly. In fact all of the slots can be cut without sharpening the tool. Although there is insufficient space to describe the procedure here, it is important to realise that the tools have to be made with the appropriate clearance angles on their faces.

To develop the procedure we manufactured a 500GHz horn which had an aperture diameter of 5mm and a length of 19mm. The waveguide measured 250μm by 500μm. The first groove at the throat was 300μm deep and, after the first few grooves, the rest of the grooves were 160μm deep. The slots were 100μm wide and had a wall thickness of 67μm. The whole operation turned out to be very fast, and each side of the mixer (100 corrugations) took about a day to machine. At this stage, the horn was, of course,

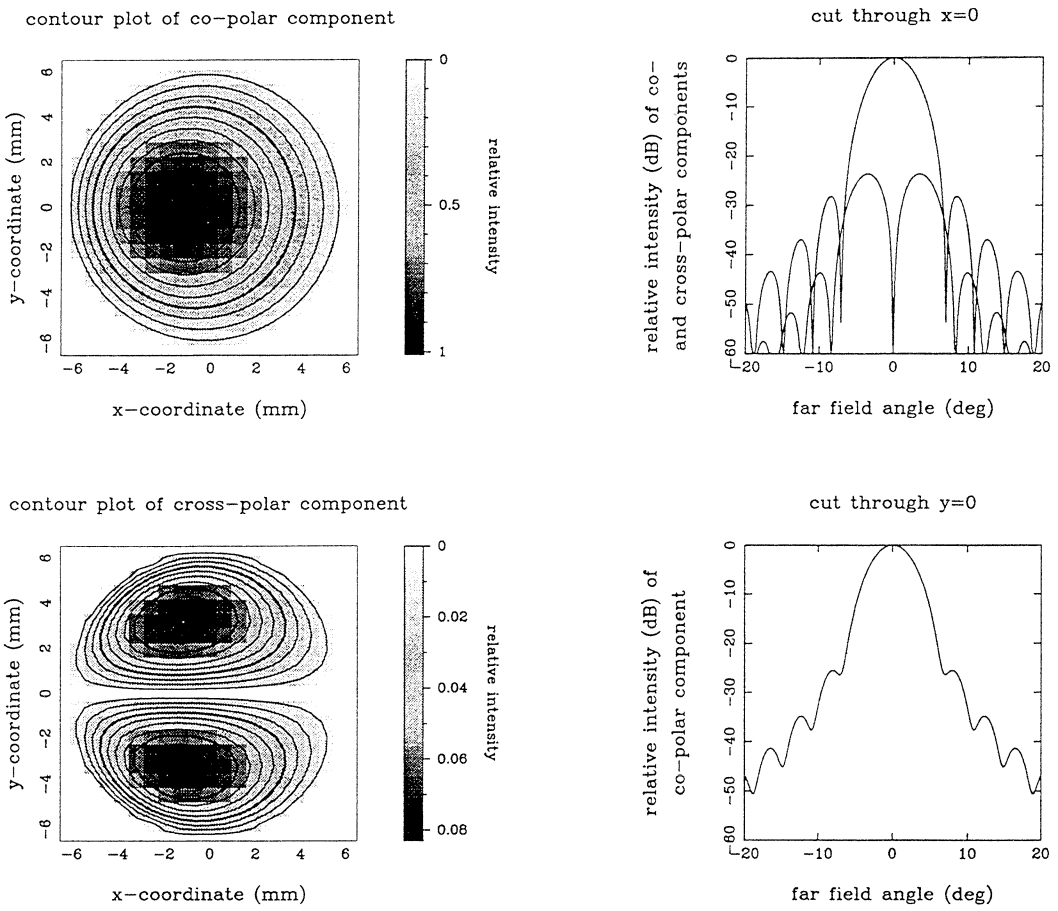

Figure 6: The co-polar and cross-polar fields in the projected aperture of a 345GHz horn having an aperture radius of 5mm and a length of20mm. The co-polar and cross-polar far-field power patterns are also shown.

complete and there was no need for electroforming.

7 Conclusions

In this paper, we have described a horn-reflector antenna which is ideal for making high-performance submillimetre-wave extragalactic imaging arrays. We have presented a theory which allows the Gaussian-mode behaviour of the antenna to be calculated. The theory has been verified by comparing the results of simulations with experimental measurements made on a horn at 17GHz.

A novel technique has been described whereby a large number of elements can be manufactured easily. There is no need for electroforming, and the block can be made out of any material, including aluminium. Because of the split-block design, the quality of the machining can be seen easily, and there are no problems with trapped electroforming fluids causing corrosion. To develop the machining techniques an antenna was made for 500GHz. There is no reason why the same technique should not be used for much shorter wavelengths.

References

[1] S. Withington, "Submillimetre-wave technology for extragalactic spectral-line astronomy," Proc. High-sensitivity radio Astronomy Conf. Univ. Manchester, January 1996.

[2] G.A. Hockham, "Investigation of a 90° corrugated horn," Electron. Lett., vol. 12, pp. 199-201, April 1976.

[3] J.N. Hines, T. Li, and R.H. Turrin, "The electrical characteristics of conical horn-reflector antenna," Bell Syst. Tech. J., vol. 42, pp. 1187-1211, July 1963.

[4] G. Yassin, M. Robson, and P.J. Duffett-Smith, "The electrical characteristics of a conical horn-reflector antenna employing a corrugated horn," IEEE Antennas Propagat., vol. AP-41, pp. 357, 1993.

[5] S. Withington and J.A. Murphy, "Multimode Gaussian Optics," Proc. 3rd International Workshop on Terahertz Electronics, Zermatt, August, 1995.